Available online at www.sciencedirect.com
SCIENCE DIRECT®
Comput. Methods Appl. Mech. Engrg. 193 (2004) 3419–3429
Computer methods in applied mechanics and engineering
www.elsevier.com/locate/cma

Defect nucleation in carbon nanotubes under tension and torsion: Stone–Wales transformation

H. Jiang [a], X.-Q. Feng [b], Y. Huang [a,*], K.C. Hwang [b], P.D. Wu [c]

[a] *Department of Mechanical and Industrial Engineering, University of Illinois, Urbana, IL 61801, USA*
[b] *Department of Engineering Mechanics, Tsinghua University, Beijing 100084, China*
[c] *Kingston Research and Development Center, Alcan International Limited, Kingston, Ont., Canada K7L 5L9*

Received 1 April 2003; received in revised form 7 August 2003; accepted 4 September 2003

Abstract

We have developed a hybrid continuum/atomistic model to study Stone–Wales transformation in single wall carbon nanotubes. The atoms far away from the defect are characterized by an atomistic-based continuum theory established from the interatomic potential, while atom positions in the vicinity of the defect are determined by molecular mechanics coupled with the atomistic-based continuum theory. For a carbon nanotube in tension, the hybrid continuum/atomistic model predicts a critical strain 4.95% for Stone–Wales transformation, which is in excellent agreement with prior molecular dynamic studies. For a carbon nanotube in torsion, the present study predicts a critical shear strain of 12%.

Keywords: Carbon nanotube; Defects; Hybrid continuum/atomistic model; Interatomic potential

1. Introduction

Atomistic studies have suggested that carbon nanotubes (CNTs) possess unique and superior electrical, electromechanical, and mechanical properties, and therefore have many potential applications such as nanoelectronics, nanoelectro-mechanical systems (NEMS), and nanocomposites (e.g., [10,19,20,22,28]). There are, however, some discrepancies between atomistic modeling and experimental results. For example, Yakobson et al.'s [29] molecular dynamics (MD) simulations based on the empirical interatomic potential for carbon [5] suggested that the breaking strain of a single wall CNT is as large as 55%, while the fracture strain of multiwall CNTs measured by [30] is less than 12%. One important reason for this large difference is that most atomistic studies have not accounted for the effect of defects in CNTs.

* Corresponding author. Tel.: +1-217-265-5072; fax: +1-217-244-6534.
E-mail address: huang9@uiuc.edu (Y. Huang).

0045-7825/$ - see front matter
doi:10.1016/j.cma.2003.09.025

Defects in CNTs can be categorized to three groups [9]:

1. *topological defects*, such as the so-called Stone–Wales transformation (i.e., 90° rotation of a C–C bond, resulting a low energy 5–7–7–5 ring pair);
2. *rehybridization defects*, which refer to the change from sp^2 to sp^3 of a C–C bond due to highly localized deformation; and
3. *incomplete bonding and other defects*, such as impurity attachments and substitutions.

The experimental studies on topological defects have mainly focussed on the change of CNT electrical properties due to defect nucleation [1,6,14,15,24,26]. For example, Tekleab et al. [24] observed abrupt change of electrical properties in the scanning tunneling microscopy and spectroscopy study of deformed CNTs. Their MD simulations suggested that this abrupt change of electrical properties can be attributed to the Stone–Wales transformation induced by large deformation.

There are some atomistic studies on topological defects in CNTs. Terrones et al. [25] investigated the structural stability of defects and the effect of defects on electrical and mechanical properties of CNTs. Nardelli et al.'s [17,18] MD simulations showed that defect nucleation in CNTs under tension occurs via Stone–Wales transformation at a critical strain between 5% and 6%. Due to the intrinsic limit on the timescale (10^{-12} s) of MD simulations, Nardelli et al. [17,18] used an extremely high strain rate of 1.7×10^{10} s^{-1} and very high temperature of 1800 K in the atomistic studies. Belytschko et al. [3] and Dumitrica et al. [8] studied fracture and bond breaking in carbon nanotubes.

The propose of this paper is to study defect nucleation in the form of Stone–Wales transformation in CNTs under quasistatic loading and low temperature. Instead of using MD which have an intrinsic limit on the timescale (10^{-12} s), we conduct a hybrid continuum/atomistic study. Atoms far away from the defect are represented by an atomistic-based continuum theory [11,31–33], which has been shown to agree well with MD simulations studies without any parameter fitting. For atoms near the defect, we use molecular mechanics coupled with the atomistic-based continuum theory to determine the atom positions. This hybrid continuum/atomistic study significantly reduces the computation. For example, for a 10 nm long CNT with more than 2000 atoms, the hybrid continuum/atomistic model involves only 42 atoms but achieves the same accuracy.

In Section 2, we use the atomistic-based continuum theory to determine the atom positions in a defect-free CNT subject to tension or torsion. The atomistic-based continuum theory is then coupled with molecular mechanics calculations to study defect nucleation in a CNT in Section 3. This hybrid continuum/atomistic study involves the energy minimization of only 42 atoms, which is significantly less than the atomistic models involving more than 2000 atoms. The results for defect nucleation in a CNT under tension and torsion are presented in Section 4 and 5, respectively.

2. An atomistic-based continuum theory for single wall carbon nanotubes

2.1. The empirical interatomic potential for carbon

The empirical interatomic potential established by Brenner [5] for carbon has been widely used in the MD simulations of CNTs. The energy V stored in the atomic bond between atoms i and j is given by

$$V = V_{\mathrm{R}}(r_{ij}) - \overline{B}_{ij} V_{\mathrm{A}}(r_{ij}), \tag{1}$$

where r_{ij} is the distance between atoms i and j; V_{R} and V_{A} are the repulsive and attractive pair terms (depending only on r_{ij}), respectively, and $\overline{B}_{ij}$ represents the multi-body coupling which depends on all neighbor atoms of i and j. (Therefore V is not a pair potential depending only on the distance r_{ij}.) The

expressions of V_R, V_A, and $\overline{B}_{ij}$, given by Brenner [5], are very long and are therefore not repeated here. Detailed expressions and the parameters involved can be found in [13,33]. It should be pointed out that the cutoff distance in the empirical interatomic potential becomes irrelevant in the present study since the Stone–Wales transformation occurs way before the cutoff distance is reached.

2.2. Carbon nanotubes prior to deformation

As shown in Fig. 1, a CNT is a honeycomb lattice (Fig. 1a) rolled into a cylinder (Fig. 1b) without any stretching. It is convenient to describe the CNT orientation and diameter via the base vectors $\boldsymbol{a}_1$ and $\boldsymbol{a}_2$ of the honeycomb lattice (e.g., [21]), where $\boldsymbol{a}_1$ and $\boldsymbol{a}_2$ are vectors from atoms B to C and D to C (Fig. 1a), respectively, and B, C, and D are three nearest-neighbor atoms of the representative atom A. The chiral vector $\boldsymbol{C}_h$, which represents the circumference of the CNT in the honeycomb lattice (Fig. 1a), can be expressed in terms of base vectors by [21]

$$\boldsymbol{C}_h = n\boldsymbol{a}_1 + m\boldsymbol{a}_2, \tag{2}$$

where, without losing generality, n and m are integers, and $n \geqslant m \geqslant 0$. The pair (n, m) is called the chirality of the CNT. Carbon nanotubes can be divided to three groups based on their chiral angle θ (the angle between $\boldsymbol{C}_h$ and $\boldsymbol{a}_1$), namely zigzag ($\theta = 0°$ or equivalently $m = 0$), armchair ($\theta = 30°$, or $n = m$), and chiral CNTs ($0° < \theta < 30°$, or $n > m > 0$).

Because of the finite curvature (radius) effect of the CNT, the honeycomb lattice (Fig. 1a) unrolled from the CNT (Fig. 1b) does not have the same lattice constants, i.e., $AB \neq AC \neq AD$. Jiang et al. [13] determined these lattice constants for various CNT chiralities (n, m) by energy minimization. The positions of nearest-neighbor atoms B, C, and D with respect to the representative atom A are also determined.

2.3. Continuum description of deformed carbon nanotubes

In this section, we determine atom positions in a CNT under tension or torsion via an atomistic-based continuum theory (e.g., [13]). The deformation gradient $\boldsymbol{F} = \partial \boldsymbol{x}/\partial \boldsymbol{X}$ characterizes the deformation of a

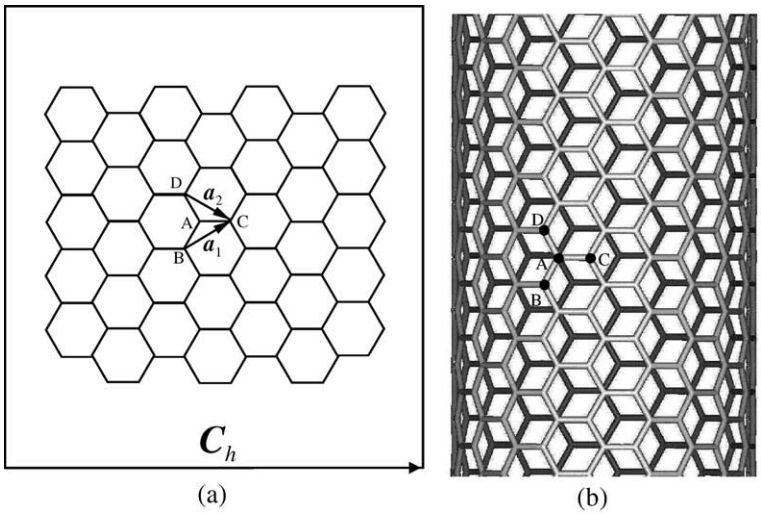

Fig. 1. A carbon nanotube (CNT) and the corresponding "unrolled" honeycomb lattice: (a) the planar, honeycomb lattice and (b) a CNT rolled from the honeycomb lattice.

material point in the continuum analysis, where the material point represents many atoms that undergo locally uniform deformation, $\boldsymbol{X}$ and $\boldsymbol{x}$ denote the positions of the material point prior to and after deformation, respectively. For a CNT subject to tension or torsion, the deformed CNT remains to have a circular cross section, and can therefore be "unrolled" to a plane. Accordingly, the deformation gradient $\boldsymbol{F}$ is intrinsically two-dimensional. This mapping from the "unrolled" plane to a cylindrical surface is similar to the method introduced by [2] which ensures that the Cauchy–Born rule is applicable to a curved surface.

Let $\boldsymbol{r}_{ij}^{(0)}$ denote the position vector from atom i to atom j prior to deformation. For a material point subject to the deformation gradient $\boldsymbol{F}$, the position vector $\boldsymbol{r}_{ij}^{(0)}$ becomes $\boldsymbol{r}_{ij} = \boldsymbol{F} \cdot \boldsymbol{r}_{ij}^{(0)}$ after the deformation. Therefore, the energy stored in the atomic bonds obtained from the empirical interatomic potential depends on $\boldsymbol{F}$. Using the Cauchy–Born rule [4,16] which equated the strain energy at the continuum level to the energy stored in atomic bonds, we obtain the strain energy density W as a function of the deformation gradient $\boldsymbol{F}$, i.e., $W = W(\boldsymbol{F})$. Such an approach, however, is limited to materials with a centrosymmetric atomic structure since the centrosymmetry together with $\boldsymbol{r}_{ij} = \boldsymbol{F} \cdot \boldsymbol{r}_{ij}^{(0)}$ ensure the equilibrium of atoms [7,23,27,32,33].

A CNT, however, does not posses centrosymmetry. As shown in Fig. 2a, a CNT prior to deformation is composed of two triangular sub-lattices (marked by open and solid circles, respectively), and each sub-lattice possesses centrosymmetry. Once the deformation is imposed, the Cauchy–Born rule discussed above can be applied to each sub-lattice, but the two sub-lattices may undergo a relative shift vector $\boldsymbol{\zeta}$, as discussed by [32,33] and shown in Fig. 2b. This shift vector $\boldsymbol{\zeta}$ plays the role of relaxing the atoms between two sub-lattices in order to ensure the equilibrium of atoms [7,23,27,33]. The position vector $\boldsymbol{r}_{ij}$ between atoms i and j from two different sub-lattices then becomes

$$\boldsymbol{r}_{ij} = \boldsymbol{F} \cdot \boldsymbol{r}_{ij}^{(0)} + \boldsymbol{\zeta}, \tag{3}$$

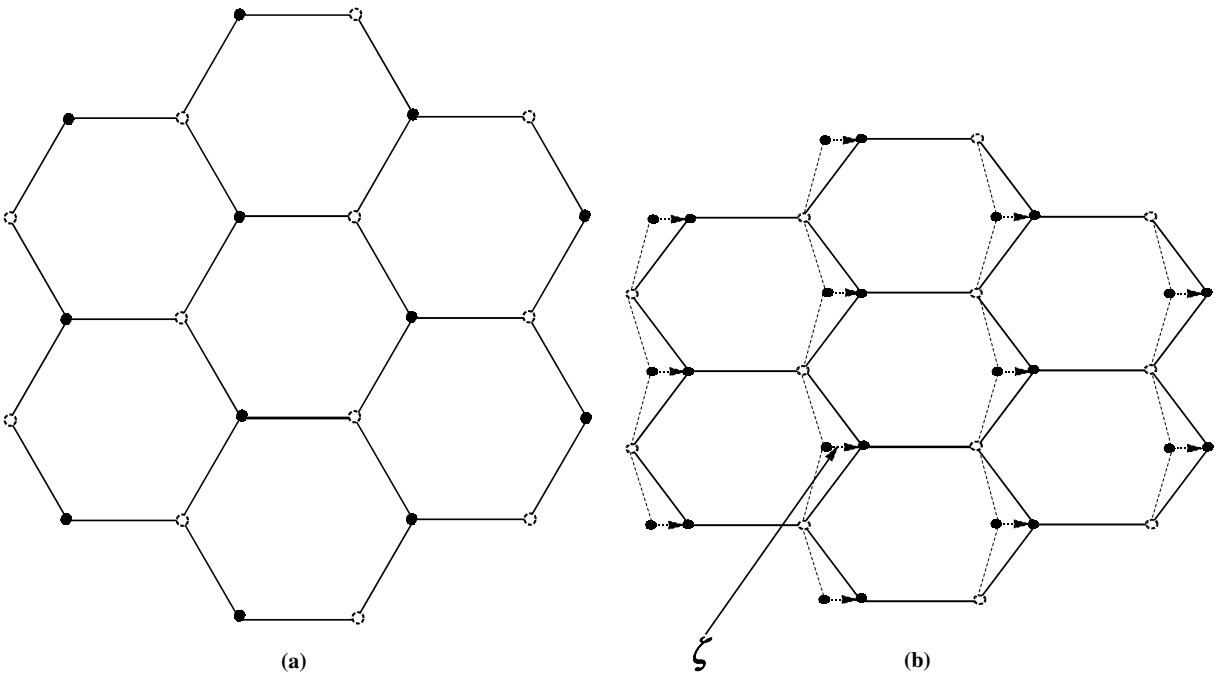

Fig. 2. (a) The decomposition of a hexagonal lattice to two triangular sub-lattices and (b) a shift vector $\boldsymbol{\zeta}$ between two sub-lattices is introduced to ensure the equilibrium of atoms. The solid and dashed lines denote the lattice structures with and without the shift vector $\boldsymbol{\zeta}$, respectively.

and their distance is

$$r_{ij} = \|r_{ij}\| = \sqrt{\boldsymbol{\zeta}\cdot\boldsymbol{\zeta} + 2\boldsymbol{\zeta}\cdot\boldsymbol{F}\cdot\boldsymbol{r}_{ij}^{(0)} + \boldsymbol{r}_{ij}^{(0)}\cdot\boldsymbol{F}^{\mathrm{T}}\cdot\boldsymbol{F}\cdot\boldsymbol{r}_{ij}^{(0)}}. \tag{4}$$

The energy stored in the atomic bonds obtained from the interatomic potential in Eq. (1) now depends on both $\boldsymbol{F}$ and $\boldsymbol{\zeta}$. The Cauchy–Born rule then gives the strain energy density W in the continuum analysis in terms of $\boldsymbol{F}$ and $\boldsymbol{\zeta}$, i.e., $W = W(\boldsymbol{F}, \boldsymbol{\zeta})$. The shift vector $\boldsymbol{\zeta}$ is determined by energy minimization which is equivalent to the equilibrium of atoms, i.e.,

$$\frac{\partial W}{\partial \boldsymbol{\zeta}} = 0. \tag{5}$$

This is an implicit equation to determine the shift vector $\boldsymbol{\zeta}$ in terms of $\boldsymbol{F}$, i.e., $\boldsymbol{\zeta} = \boldsymbol{\zeta}(\boldsymbol{F})$. The strain energy density then becomes

$$W = W[\boldsymbol{F}, \boldsymbol{\zeta}(\boldsymbol{F})]. \tag{6}$$

The second Piola–Kirchhoff stress $\boldsymbol{T}$ is the work conjugate of the Lagrangian strain $\boldsymbol{E} = \frac{1}{2}(\boldsymbol{F}\cdot\boldsymbol{F} - \boldsymbol{I})$, i.e., $\boldsymbol{T} = \partial W/\partial \boldsymbol{E}$, where $\boldsymbol{F}^T$ is the transpose of $\boldsymbol{F}$ and $\boldsymbol{I}$ is the second-order identity tensor.

3. Deformation-induced Stone–Wales transformation in a carbon nanotube

The MD simulations of Nardelli et al. [17,18] showed that the Stone–Wales transformation occurred in a CNT under tension at about 5% tensile strain. The MD simulations, however, are limited on both the timescale (10^{-12} s) and length scale. For example, a 10 nm long, $(10, 10)$ CNT involves more than 2000 atoms, and its atomistic study is computationally intensive. On the other hand, the effect of Stone–Wales transformation, which involves the 90° rotation of a carbon bond, is rather local and limited to atoms in the neighborhood of defect nucleation. Atoms far away from the defect undergo uniform deformation, and we may use the atomistic-based continuum theory described in Section 2 to determine their positions. For atoms near the defect, we use molecular mechanics coupled with the atomistic-based continuum theory.

Fig. 3a and b illustrate our hybrid continuum/atomistic model to study the Stone–Wales transformation in a CNT. Only the "unrolled" honeycomb lattice is shown, but all calculations are done for the cylindrical configuration of the CNT. As the strain in the CNT reaches a critical value, a carbon bond rotates 90°, the so-called Stone–Wales transformation forming two pentagons and two heptagons which is called the 5–7–7–5 ring pair. The rotated bond prior to and after the transformation are highlighted in Fig. 3a and b, respectively. The atoms can be divided to two groups as shown in Fig. 3a and b. Those in the vicinity of the defect are marked by the shaded circles, while atoms away from the defect are marked by open and solid circles which is consistent with Fig. 2 to represent atoms from two sub-lattices. Atoms in the latter group undergo relatively uniform deformation since the effect of bond rotation is rather localized. Therefore, the positions of these atoms (far ways from the defect) can be determined by the atomistic-based continuum theory. (Here we have neglected the effect of Stone–Wales transformation on atoms far away.) Once the positions of atoms in the latter group are known, the positions of atoms in the former group (i.e., in the vicinity of the defect) are determined by molecular mechanics calculations to minimize energy in the system. Here we use the conjugate gradient method in the IMSL. Program [12] to minimize the energy with respect only to positions of atoms in the former group (i.e., the shaded circles in the vicinity of defect), though it is important to account for the energy stored in the atomic bonds across these two different groups of atoms (i.e., from shaded circles to open or solid circles in Fig. 3) in the molecular mechanics calculations. Such an approach involves both continuum and atomistic calculations, and is therefore called a hybrid continuum/atomistic model in the following.

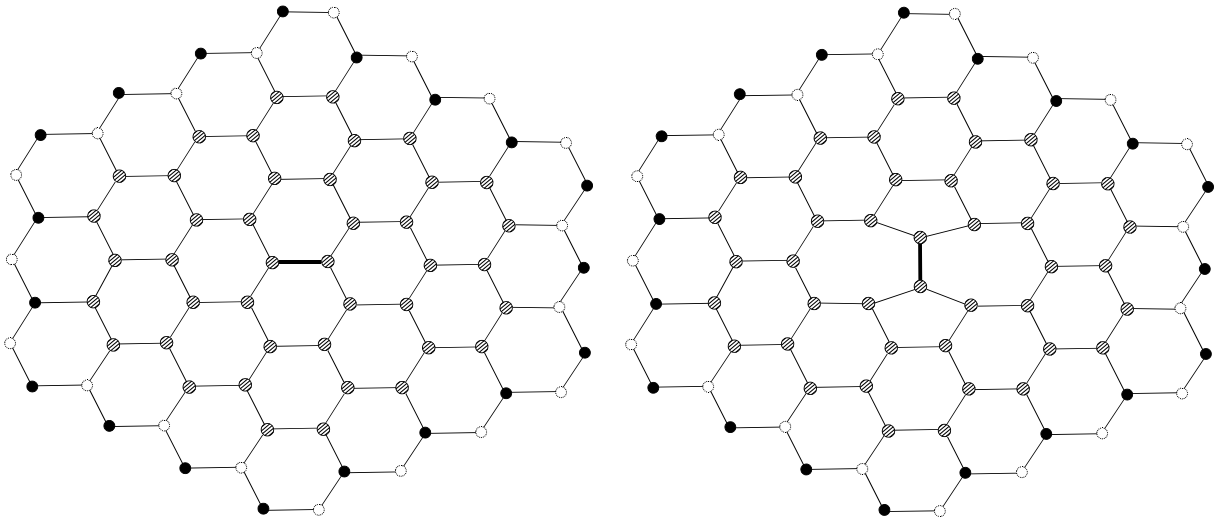

Fig. 3. A hybrid continuum/atomistic model to study the Stone–Wales transformation in a carbon nanotube. The open and solid circles denote atoms whose positions are determined by the atomistic-based continuum theory, while the shaded circles represent atoms whose positions are determined by the hybrid continuum/atomistic model: (a) without the Stone–Wales transformation and (b) with the Stone–Wales transformation.

We use the above hybrid continuum/atomistic model to calculate the energy E_{perfect} in the system without the defect (Fig. 3a) and the energy E_{defect} with a per-existing defect (Fig. 3b) in the form of Stone–Wales transformation (i.e, 90° rotation of a carbon bond). Both E_{perfect} and E_{deffect} depend on the deformation gradient $\boldsymbol{F}$ in the CNT, but E_{defect} is always larger at infinitesimal strain because of the defect. As the strain increase, E_{defect} may become smaller (i.e., $E_{\text{defect}} < E_{\text{perfect}}$), the Stone–Wales transformation then becomes more energetically favorable, and defect nucleation may occur (though this criterion $E_{\text{defect}} < E_{\text{perfect}}$ has not accounted for kinetics of defect formation).

In order to ensure the hybrid continuum/atomistic model gives accurate results, there should be sufficient number of atoms in the former group, i.e., in the vicinity of the defect. We have used 42 atoms (as shown in Fig. 3) as well as 80 atoms around the defect in the molecular mechanics calculations, and the results are the same.

4. Stone–Wales transformation in tension

For a CNT in simple tension, Nardelli et al.'s [17,18] MD simulation predicted that the Stone–Wales transformation occurred at the tensile strain around 5%. We use the hybrid continuum/atomistic model to study the Stone–Wales transformation in tension. There are two non-vanishing components of the deformation gradient, F_{ZZ} and $F_{\Theta\Theta}$, and they are related by the uniaxial tension condition $T_{\Theta\Theta} = 0$, where Z and Θ denote the axial and circumferential directions, respectively, and $T_{\Theta\Theta}$ is the second Piola-Kirchhoff stress. For each given axial strain $\epsilon_{ZZ} = F_{ZZ} - 1$ (i.e., percent increase of CNT length), the hybrid continuum/atomistic model in the previous section gives the energy E_{perfect} and E_{defect} for the system without and with the defect, respectively. The energy versus the axial strain ϵ_{ZZ} is shown in Fig. 4 for both perfect and defect-containing $(10, 10)$ CNTs. Here the CNT without the defect at zero strain is taken as the ground state (i.e., zero energy). For the perfect $(10, 10)$ CNT, the energy increases monotonically with the strain.

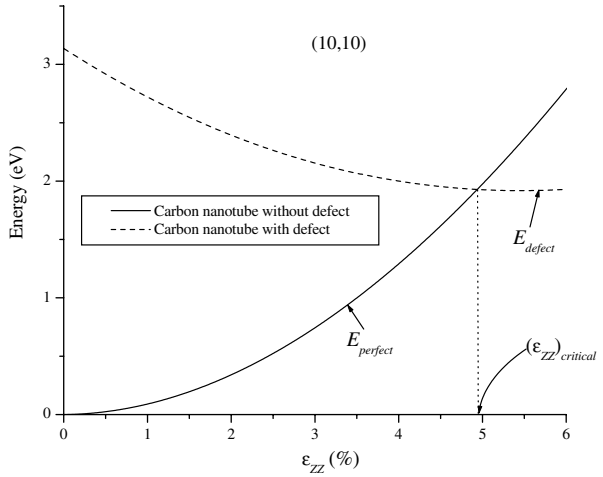

Fig. 4. Energy versus axial strain ϵ_{ZZ} for perfect and defect-containing $(10, 10)$ carbon nanotubes in tension.

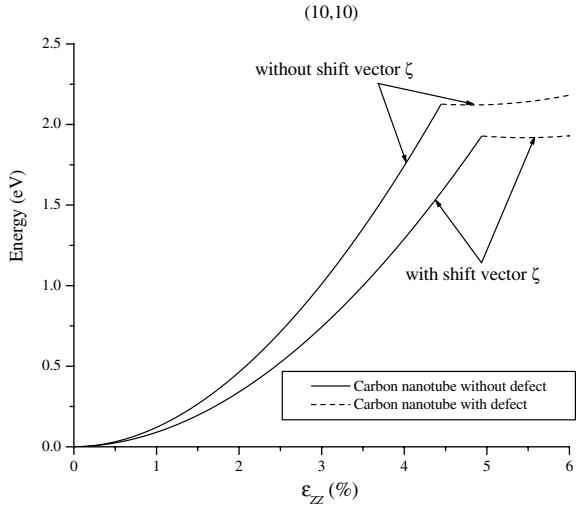

Fig. 5. Energy versus axial strain ϵ_{ZZ} for a carbon nanotube in tension with and without the shift vector $\boldsymbol{\zeta}$.

For the defect-containing $(10, 10)$ CNT, there is a finite energy at zero strain because of the defect, and the energy decreases as the strain increases. Below a critical axial strain $(\epsilon_{ZZ})_{\text{critical}} = 4.95\%$ at which $E_{\text{defect}} = E_{\text{perfect}}$, the perfect CNT has lower energy and is therefore energetically favorable. Once the axial strain exceeds this critical value of 4.95%, the energy in the defect-containing CNT is lower such that defect nucleation becomes more energetically favorable. This critical axial strain of 4.95% agrees well with Nardelli et al.'s [17,18] MD simulations which reported the critical strains triggering the Stone–Wales transformation around 5%.

The shift vector $\boldsymbol{\zeta}$, which was introduced in atomistic-based continuum theory in Section 2 to ensure the equilibrium of atoms, has an important effect on the present hybrid continuum/atomistic study of Stone–Wales transformation in a CNT. The curve of energy versus the axial strain ϵ_{ZZ} without accounting for the shift vector is compared with that accounting for such effect in Fig. 5, and the latter

Table 1
Effect of tube diameter on the critical strains for Stone–Wales transformation in carbon nanotubes in tension and torsion

Chirality (n, m)	Chiral angle (°)	Diameter (nm)	Critical axial strain $(\epsilon_{ZZ})_{\text{critical}}$ (%) in tension	Critical shear strain $(\kappa R)_{\text{critical}}$ (%) in torsion
$(6, 6)$	30.00	0.84	4.70	11.94
$(8, 8)$	30.00	1.11	4.92	12.21
$(10, 10)$	30.00	1.39	4.95	12.21
$(12, 12)$	30.00	1.66	4.97	12.22
$(15, 15)$	30.00	2.08	5.01	12.24
$(18, 18)$	30.00	2.50	5.04	12.24
$(20, 20)$	30.00	2.77	5.04	12.24

Table 2
Effect of chiral angle on the critical strains for Stone–Wales transformation in carbon nanotubes in tension and torsion

Chirality (n, m)	Chiral angle (°)	Diameter (nm)	Critical axial strain $(\epsilon_{ZZ})_{\text{critical}}$ (%) in tension	Critical shear strain $(\kappa R)_{\text{critical}}$ (%) in torsion
$(17, 0)$	0.00	1.36	6.72	7.98
$(17, 1)$	2.83	1.40	6.31	8.10
$(16, 2)$	5.82	1.37	5.99	8.37
$(16, 3)$	8.45	1.42	5.81	8.58
$(15, 4)$	11.53	1.39	5.58	8.91
$(14, 5)$	14.71	1.37	5.49	9.15
$(13, 6)$	18.00	1.35	5.20	9.75
$(13, 7)$	20.17	1.41	5.12	10.11
$(12, 8)$	23.41	1.37	5.05	10.77
$(11, 9)$	26.70	1.39	4.98	11.40
$(10, 10)$	30.00	1.39	4.95	12.21

is the same as the curve in Fig. 4. It is observed that, without accounting for the shift vector, the hybrid continuum/atomistic model predicts higher energy, and lower critical strain of $\epsilon_{ZZ} = 4.44\%$ for defect nucleation.

Table 1 shows the critical strain for several armchair CNTs that have the same chiral angle (angle between $\boldsymbol{C}_{\text{h}}$ and $\boldsymbol{a}_1$ in Fig. 1) but different tube diameters ranging from 0.84 to 2.77 nm. The variation of critical strain is rather small, from 4.70% to 5.04%. This suggests that the CNT diameter does not have a significant effect on Stone–Wales transformation. The chiral angle, however, has somewhat larger effect. Table 2 shows the critical strain for several CNTs under tension that have approximately the same diameter around 1.38 nm but different chiral angles. The critical strain ranges from 4.95% for an armchair $(10, 10)$ CNT to 6.72% for a zigzag $(17, 0)$ CNT. For the same CNT diameter, the zigzag CNT requires a larger critical strain for Stone–Wales transformation than the armchair CNT.

5. Stone–Wales transformation in torsion

The good agreement between the hybrid continum/atomistic model and Nardelli et al.'s [17,18] MD simulations on the critical strain for Stone–Wales transformation in CNTs under tension provides validation of the proposed approach. To the best of our knowledge, there are no MD simulations on Stone–Wales transformation in CNTs under torsion. We use the hybrid continuum/atomistic model to predict the critical shear strain triggering the Stone–Wales transformation in pure torsion.

Let κ denote the twist (angle of rotation per unit length) for a CNT in pure torsion; (R, Θ, Z) and (r, θ, z) be the cylindrical coordinates of a material point on the CNT prior to and after the deformation, respectively, and they are related by $\theta = \Theta + \kappa Z$ and $z = (1 + \epsilon)Z$, with ϵ being the axial strain due to the finite rotation. The corresponding base vectors are denoted by $(\boldsymbol{e}_{\mathrm{R}}, \boldsymbol{e}_{\Theta}, \boldsymbol{e}_z)$ and $(\boldsymbol{e}_{\mathrm{r}}, \boldsymbol{e}_{\theta}, \boldsymbol{e}_z)$. The deformation gradient in pure torsion is given by

$$\boldsymbol{F} = \frac{r}{R} e_{\theta} \boldsymbol{e}_{\Theta} + \kappa r \boldsymbol{e}_{\theta} e_Z + (1 + \varepsilon) \boldsymbol{e}_z \boldsymbol{e}_Z. \tag{7}$$

The equilibrium equation and boundary conditions in pure torsion require the normal stress tractions to vanish, which gives [13]

$$T_{\Theta\Theta} = -2\kappa R T_{\Theta Z}, \quad T_{ZZ} = 0. \tag{8}$$

The radius r of the deformed CNT and the axial strain ϵ are determined from (8) in terms of the twist κ.

We use the hybrid continuum/atomistic model in Section 3 to calculate the energy E_{perfect} and E_{defect} for the system without and with the defect, respectively. Fig. 6 shows the energy versus the shear strain κR for a $(10, 10)$ CNT in torsion. Similar to Fig. 4 for simple tension, the energy E_{perfect} increases monotonically with κR in torsion, while E_{deffect} initially decreases and then increases with κR. The critical shear strain at which $E_{\mathrm{perfect}} = E_{\mathrm{deffect}}$ is found to be $(\kappa R)_{\mathrm{critical}} = 0.12$. Therefore, for $\kappa R > 0.12$, the CNT with the Stone–Wales transformation is more energetically favorable than the CNT without the defect.

The critical shear strain $(\kappa R)_{\mathrm{critical}}$ shown in Tables 1 and 2 for the Stone–Wales transformation in CNTs under torsion confirm the conclusion established in the previous section that the CNT diameter has little effect on the Stone–Wales transformation, but the chiral angle has a larger effect. However, contrary to CNTs under tension, the critical strain for Stone–Wales transformation is smaller for a zigzag CNT [e.g., $(17, 0)$] than that for an armchair CNT [e.g., $(10, 10)$]. This opposite dependence on the chiral angle is due to different bond orientations with respect to the loading direction in tension and torsion.

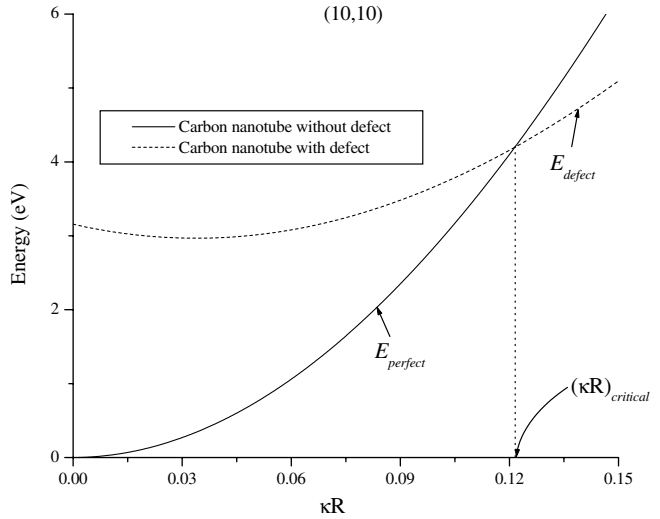

Fig. 6. Energy versus shear strain κR for perfect and defect-containing carbon nanotubes in torsion.

6. Concluding remarks

We have proposed a hybrid continuum/atomistic model to study the Stone–Wales transformation in carbon nanotubes. The position of atoms far away from the defect are determined by an atomistic-based continuum model established from the interatomic potential. The positions of atoms near the defect are determined by molecular mechanics calculations coupled with the atomistic-based continuum model. For a carbon nanotube in tension, the critical strain for the Stone–Wales transformation predicted by the hybrid continuum/atomistic model agrees very well with molecular dynamic simulations. We have also calculated the critical shear strain for Stone–Wales transformation in a carbon nanotube under torsion.

Acknowledgements

Y.H. acknowledges the support from NSF (grants 00-99909 and 01-03257 and NSF–CEMMS Center at UIUC), Alexander von Humboldt Foundation, Center for Advanced Study at the University of Illinois, Urbana-Champaign, the NCSA/UIUC Faculty Fellow Program, and NSFC. X.Q.F. and K.C.H. acknowledge the support from NSFC.

References

[1] S. Amelinckx, X.B. Zhang, D. Bernaerts, X.F. Zhang, V. Ivanov, J.B. Nagy, A formation mechanism for catalytically grown helix-shaped graphite nanotubes, Science 265 (1994) 635–639.
[2] M. Arroyo, T. Belytschko, An atomistic-based finite deformation membrane for single layer crystalline films, J. Mech. Phys. Solids 50 (2002) 1941–1977.
[3] T. Belytschko, S.P. Xiao, G.C. Schatz, R.S. Ruoff, Atomistic simulations of nanotube fracture, Phys. Rev. B 65 (2002) 1–8.
[4] M. Born, K. Huang, Dynamical theory of the crystal lattices, Oxford University Press, Oxford, 1954.
[5] D.W. Brenner, Empirical potential for hydrocarbons for use in simulating the chemical vapor deposition of diamond films, Phys. Rev. B 42 (1990) 9458–9471.
[6] D.L. Carroll, P. Redlich, P.M. Ajayan, J.C. Charlier, X. Blase, A.D. Vita, R. Car, Electronic structure and localized states at carbon nanotube tips, Phys. Rev. Lett. 78 (1997) 2811–2814.
[7] C. Cousins, Inner elasticity, J. Phys. C 11 (1978) 4867–4879.
[8] T. Dumitrica, T. Belytschko, B.I. Yakobson, Bond-breaking bifurcation states in carbon nanotube fracture, J. Chem. Phys. 118 (2003) 9485–9488.
[9] T.W. Ebbesen, T. Takada, Topological and sp^3 defect structures in nanotubes, Carbon 33 (1995) 973–999.
[10] S. Govindjee, J.L. Sackman, On the use of continuum mechanics to estimate the properties of nanotubes, Solid State Commun. 110 (1999) 227–230.
[11] Y. Huang, Z.L. Wang, Mechanics of carbon nanotubes, in: B. Karihaloo, R. Ritchie, I. Milne (Eds.), Comprehensive Structural Integrity Handbook, Vol. 8 of Interfacial and Nanoscale Fracture (volume editors W. Gerberwich, W. Yang), Elsevier, Amsterdam, 2003, chapter 8.16, pp. 551–579.
[12] IMSL(R) Fortran 90 MP Library Version 4.01. McGraw-Hill, San Ramon, 1999.
[13] H. Jiang, P. Zhang, B. Liu, Y. Huang, P.H. Geubelle, H. Gao, K.C. Hwang, The effect of nanotube radius on the constitutive model for carbon nanotubes, Computat. Mater. Sci. 28 (2003) 429–442.
[14] P. Kim, T.W. Odom, J. Huang, C.M. Lieber, Electronic density of states of atomically resolved single-walled carbon naotubes: Van Hove singularities and end states, Phys. Rev. Lett. 82 (1999) 1225–1228.
[15] V. Meunier, P. Lambin, Scanning tunneling microscopy and spectroscopy of topological defects in carbon nanotubes, Carbon 38 (2000) 1729–1733.
[16] F. Milstein, Review: theoretical elastic behaviour at large strains, J. Mater. Sci. 15 (1980) 1071–1084.
[17] M.B. Nardelli, B.I. Yakobson, J. Bernholc, Brittle and ductile behavior in carbon nanotubes, Phys. Rev. Lett. 81 (1998) 4656–4659.
[18] M.B. Nardelli, B.I. Yakobson, J. Bernholc, Mechanism of strain release in carbon nanotubes, Phys. Rev. B 57 (1998) R4277–R4280.
[19] D. Qian, G.J. Wagner, W.K. Liu, M.-F. Yu, R.S. Ruoff, Mechanics of carbon nanotubes, Appl. Mech. Rev. (2002).

[20] R.S. Ruoff, D.C. Lorents, Mechanical and thermal properties of carbon nanotubes, Carbon 33 (1995) 925–930.
[21] R. Saito, G. Dresselhaus, M.S. Dresselhaus, Physical Properties of Carbon Nanotubes, Imperial College Press, London, 1998.
[22] D. Srivastava, M. Menon, K.J. Cho, Computational nanotechnology with carbon nanotubes and fullerenes, Comput. Sci. Engrg. 3 (2001) 42–55.
[23] E.B. Tadmor, G.S. Smith, N. Bernstein, E. Kaxiras, Mixed finite element and atomistic formulation for complex crystals, Phys. Rev. B 59 (1999) 235–245.
[24] D. Tekleab, D.L. Carroll, G. Samsonidze, B.I. Yakobson, Stain-induced electronic property heterogeneity of a carbon nanotube, Phys. Rev. B 64 (2001) 035419-1–035419-5.
[25] H. Terrones, M. Terrones, E. Hernández, N. Grobert, J.-C. Charlier, P.M. Ajayan, New metallic allotropes of planar and tubular carbon, Phys. Rev. Lett. 84 (2000) 1716–1719.
[26] M. Terrones, W.K. Hsu, J.P. Hare, H.W. Kroto, H. Terrones, D.R.M. Walton, Graphitic structures: from planar to spheres toroids and helices, Philos. Trans. R. Soc. London Ser. A 354 (1996) 2025–2054.
[27] J.H. Weiner, Statistical Mechanics of Elasticity, John Wiley and Sons, New York, 1983.
[28] B.I. Yakobson, P. Avouris, Mechanical properties of carbon nanotubes, in: M.S. Dresselhaus, G. Dresselhaus, P. Avouris (Eds.), Carbon Nanotubes, Topics in Applied Physics, vol. 80, 2001.
[29] B.I. Yakobson, M.P. Campbell, C.J. Brabec, J. Bernholc, High strain rate fracture and C-chain unraveling in carbon nanotubes, Computat. Mater. Sci. 8 (1997) 341–348.
[30] M.-F. Yu, O. Lourie, M.J. Dyer, K. Moloni, T.F. Kelly, R.S. Ruoff, Strength and breaking mechanism of multiwalled carbon nanotubes under tensile load, Science 287 (2000) 637–640.
[31] P. Zhang, Y. Huang, H. Gao, K.C. Hwang, Fracture nucleation in single-wall carbon nanotubes under tension: a continuum analysis incorporating interatomic potentials, J. Appl. Mech. 69 (2002) 454–458.
[32] P. Zhang, Y. Huang, P.H. Geubelle, K.C. Hwang, On the continuum modeling of carbon nanotubes, Acta Mech. Sin. 18 (2002) 528–536.
[33] P. Zhang, Y. Huang, P.H. Geubelle, P.A. Klein, K.C. Hwang, The elastic modulus of single-wall carbon nanotubes: a continuum analysis incorporating interatomic potentials, Int. J. Solids Struct. 39 (2002) 3893–3906.